ADVANCED MATERIALS

DOI: 10.1002/adma.200600606

Electrodeposition of Thermoelectric Superlattice Nanowires**

By *Bongyoung Yoo*, *Feng Xiao*, *Krassimir N. Bozhilov*, *Jennifer Herman*, *Margaret A. Ryan*, and *Nosang V. Myung**

There is a renewed interest in the field of thermoelectrics because of the remarkable efficiency improvement that can be achieved in nanostructured materials,[1] for example, superlattice thin films[2,3] and quantum dots.[4] Theoretical calculations predict that further enhancement of the thermoelectric figure of merit can be achieved in superlattice nanowires (zero-dimensional) [5] rather than conventional nanowires (1D) or superlattice thin-films (2D). In superlattice nanowires, a reduction of the thermal conductivity, which is related to phonon scattering at the interfaces between periodically alternating materials, could be achieved by controlling the diameter and length of the individual segments of the nanowires.[6] In addition, the band offset between segments provides both higher quantum confinement as well as a sharper density of electronic states compared to nanowires.

Recently, superlattice nanowires have been fabricated by a variety of methods.[7–9] For example, Si/SiGe[7] and GaAs/GaP[8] superlattice nanowires were synthesized by a laser-assisted catalytic growth method. Electrodeposition is a promising alternative technique for the fabrication of superlattice nanowires because it is simple, inexpensive, fast, operates at near room-temperature, and is able to tailor the properties of the deposit by adjusting the deposition conditions. For example, Fert et al.[10] fabricated Co/Cu superlattice nanowires from a single sulfate bath containing both metal ions by using a template-directed method that utilized the different deposition potentials of Co and Cu. By alternating the deposition potentials and deposition times, superlattice nanowires with controlled compositions and lengths were fabricated. Using a similar method, Co/Pt superlattice nanowires were also reported.[11] Even though there are several studies on the electrodeposition of thermoelectric nanowires,[12–16] thermoelectric superlattice nanowires have not yet been reported.

In this study, we electrodeposited $Bi_2Te_3/(Bi_{0.3}Sb_{0.7})_2Te_3$ superlattice nanowires by using a template-directed method, where the composition of the segments was controlled by manipulation of the deposition potential. BiTe/BiSbTe superlattice nanowires were chosen because BiTe and its derivative compounds are considered to be the best materials for thermoelectric refrigeration at room temperature. In the electrochemical deposition of alloys from aqueous electrolytes, the composition of the deposit can be manipulated by varying the applied potential, because the reduction potential of each ion in the solution is different. Therefore, a periodically modulated composition can be obtained, with two different phases forming the nanowire (e.g., Sb-rich BiSbTe and BiTe with minimal incorporation of Sb), by applying an alternating potential. Characterization of the composition and microstructure was performed to verify the synthesis of $Bi_2Te_3/(Bi_{0.3}Sb_{0.7})_2Te_3$ superlattice nanowires.

Based on previous work, BiSbTe ternary alloys can be deposited from various acidic baths with the use of complexing agents such as tartaric acid[13,17] or ethylenediaminetetraacetic acid (EDTA)[18] to solubilize Sb in water. In this study, tartaric acid (33 mM) was used as a complexing agent. Because of the low-pH operating conditions, the effect of tartaric acid on the electrodeposition was minimal. To successfully achieve compositional modulation in the BiTe/BiSbTe nanowires, the composition as a function of applied potential was first studied in order to determine the deposition potential necessary for obtaining BiSbTe alloys with different compositions. Initially, linear-sweep voltammetry (LSV) was performed to determine the deposition potential range. As shown in Figure 1a, three reduction waves were observed. The first reduction wave (C_1) extends from 100 mV to –40 mV (versus the saturated calomel electrode (SCE)), and it involved the reduction of $HTeO^+$ to Te^0 as well as the deposition of Bi_2Te_3.[19] This is expected because electrodeposition of Te^0 and Bi_2Te_3 is more noble than reduction of other possible products, such as Sb_xTe_y, Bi, and $Bi_xSb_yTe_z$.[16] The composition of the electrodeposit obtained at –20 mV could be evidence that the formation of Te^0 and Bi_xTe_y was the preferred reaction in this potential range. (Fig. 1b) The intermediate reduction wave (C_2) extends from –40 mV to –100 mV, and involved the formation of $Bi_xSb_yTe_3$ ternary alloys. The third reduction wave (C_3) extends from –100 mV to –280 mV, and involved the formation of $(Bi_{0.3}Sb_{0.7})_2Te_3$. As shown in Figure 1b, the amount of Sb in

[*] Prof. N. V. Myung, Dr. B. Yoo,[+] F. Xiao[+]
Department of Chemical and Environmental Engineering and
Center for Nanoscale Science and Engineering
University of California-Riverside
Riverside, CA 92521 (USA)
E-mail: myung@engr.ucr.edu
Dr. K. N. Bozhilov
Central Facility for Advanced Microscopy and Microanalysis
University of California-Riverside
Riverside, CA 92521 (USA)
J. Herman, Dr. M. A. Ryan
Electrochemical Technology Group and
Materials and Device Technology Group, Jet Propulsion Laboratory
California Institute of Technology
Pasadena, CA 91109 (USA)
[+] These authors contributed equally to this work.
[**] This work was supported by the JPL/NASA Bio/Nano program and the Korea Institute of Machinery and Materials (KIMM).

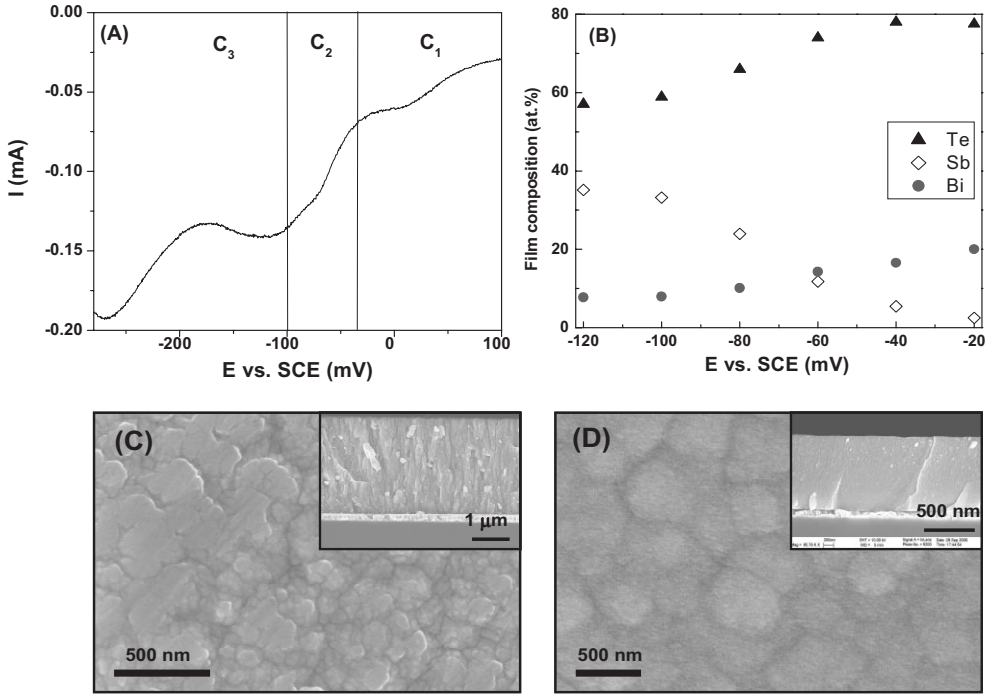

Figure 1. A) Linear-sweep voltammogram and B) film composition of BiSbTe thin film as a function of applied potential. C,D) Scanning electron microscopy (SEM) images of BiSbTe thin films deposited at –20 mV (C) and –100 mV (D). The film composition was $Bi_{2.0}Sb_{0.3}Te_{7.7}$ (approximately Bi_2Te_8) at –20 mV, and $Bi_{0.4}Sb_{1.6}Te_3$ at –100 mV, respectively. Inset images show cross-sectional views of the thin films.

the electrodeposit increased as the cathode character of the applied potential increased. The reductions of SbO^+ and Sb^{3+} to Sb^0 were expected to take place at more negative potential;[17] therefore, an increase in the Sb content of the electrodeposit in this potential range (from –40 to –100 mV) can be explained by the formation of a BiSbTe ternary alloy with increased Sb content. Figure 1c and d show scanning electron microscopy (SEM) images of BiTe and BiSbTe thin-films electrodeposited at –20 mV and –100 mV, respectively. The surface morphology of the thin films was independent of the deposition potential. At the applied potentials, the deposition rate was determined to be 0.37 nm s^{-1} at –20 mV and 1.7 nm s^{-1} at –100 mV. A cross-sectional image shows that columnar dense deposits were formed in these conditions.

From the above studies, two deposition potentials (i.e., –20 mV and –100 mV) were selected to deposit Bi_2Te_3, $(Bi_{0.3}Sb_{0.7})_2Te_3$, and their superlattice nanowires. Prior to fabrication of the superlattice, the deposition rate was determined by dividing the average length of the nanowires by the corresponding deposition times. The average length of the nanowires was confirmed from SEM images. To avoid inaccuracies in the average length of the nanowires (e.g., by breaking), the nanowires that were used for measuring the deposition rate were grown no longer than 1 μm. Interestingly, the deposition rate increased when the deposition was performed in a template. (0.6 nm s^{-1} at –20 mV, 2.6 nm s^{-1} at –100 mV) This discrepancy must have been caused by a change of mass transfer conditions inside the pores. Based on these results, superlattice nanowires with controlled compositions and length were fabricated by manipulating the applied-potential waveforms and pulse times. Typical applied-potential waveforms and their corresponding currents are shown in Figure 2.

Figure 3 shows SEM and transmission electron microscopy (TEM) images of the nanowires after removal of the polycarbonate template. The average diameter of the nanowires is approximately 50 nm, which is predetermined by the pore size of the polycarbonate membrane. Because SEM imaging cannot distinguish segments, TEM measurements were preformed to verify the structure of the superlattice nanowire (inset image in Fig. 2). As shown in the inset, bright field (BF) mass-con-

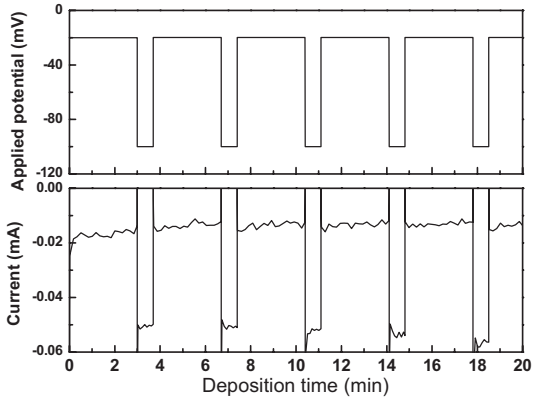

Figure 2. Applied rectangular potential pulse (top) and corresponding current response (bottom) during electrodeposition of superlattice BiSbTe nanowires.

ADVANCED MATERIALS

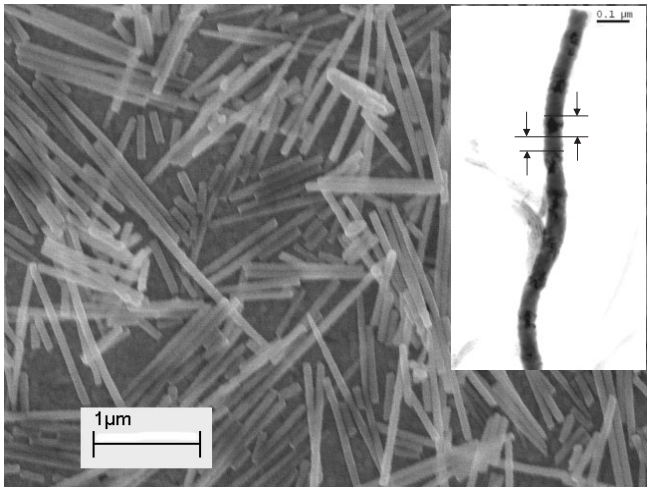

Figure 3. Microstructure of the superlattice BiSbTe nanowires after removal of the polycarbonate template. The topological image was taken by SEM, and the inset image was obtained by transmission electron microscopy (TEM). The lengths of the BiTe segments (darker regime) and BiSbTe segments (brighter regime) in the TEM image were 90 and 60 nm, respectively.

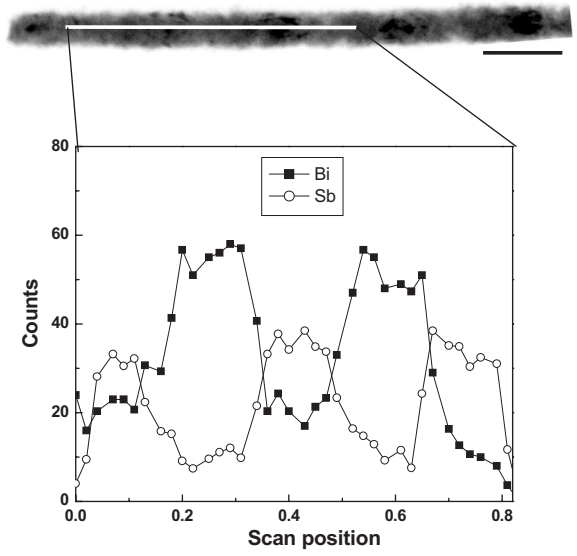

Figure 4. Energy dispersive X-ray spectrometry (EDS) line scan, showing compositional oscillations of Sb and Bi in a BiSbTe superlattice nanowire.

trast imaging by TEM clearly distinguishes the two segments of different composition by contrast. The BiTe segment, with a length of ca. 90 nm, appears darker in the TEM image, whereas the BiSbTe segment, with a length of ca. 60 nm, appears relatively lighter. The compositional modulation within the nanowires was examined by electron dispersive X-ray spectroscopy (EDS) with the line-scanning method, where the intensity of the characteristic Bi Lα and Sb Kα peaks is plotted as a function of distance (Fig. 4). The intensity of each characteristic peak is proportional to the concentration, because the nanowires have a relatively constant thickness. From the EDS intensity profiles it was clearly confirmed that Bi and Sb are effectively modulated with precise periods. The composition of each phase in the superlattice nanowire was determined to be Te-rich Bi_2Te_3 and $(Bi_{0.3}Sb_{0.7})_2Te_3$, showing that the Bi concentration in the nanowires was increased, compared to the thin-film results from Figure 1 at the same potential conditions, and that there is a discrepancy in deposition rate between the nanowires and the thin film. The differences in composition and rate of deposition between nanowires and thin films might be attributed to different mass-transport phenomena at the deposition interface.

The microstructure of the superlattice BiSbTe nanowires was investigated by electron diffraction and diffraction contrast in the TEM. Figure 5a and b shows a BF image of superlattice nanowire and a selected-area electron diffraction pattern, respectively. In the SAED pattern, ring patterns were observed, along with several strong diffraction spots, suggesting that crystals with a variety of sizes were present. The microstructure of the nanowire was revealed clearly by diffraction-contrast imaging. Figure 5c–e shows the formed TEM-centered dark-field (DF) images, with the reflections marked df1, df2, and df3, respectively.

The reflections df1 and df2 (Fig. 5a) belong to the Bi_2Te_3 phase, as evident from the DF images formed with these reflections (Fig. 5c and d), which indicated that the Bi_2Te_3 segments were composed of larger grains than the $(Bi_{0.3}Sb_{0.7})_2Te_3$ segments. The slightly diffuse ring pattern apparently resulted from the finer grains of the $(Bi_{0.3}Sb_{0.7})_2Te_3$ phase, which is demonstrated in the DF image on Figure 5e, formed with a portion of the ring intensity marked as df3. The fact that the crystal sizes of the BiTe and BiSbTe phases are substantially different (even though the BiSbTe alloy exists as a solid solution of BiTe and SbTe,[20] both of which have the same rhombohedral ($R3m$) lattice structure) and the fact that both phases were obtained from the same bath at the same pH and temperature strongly implied that the applied potential was the critical parameter for determining the crystal size. In electrodeposition, the nucleation rate increases exponentially with an increase in cathodic overpotential. Therefore, a higher applied potential could result in an increased nucleation rate, enhancing grain-size refinement.[21] As shown in Figure 1, the $(Bi_{0.3}Sb_{0.7})_2Te_3$ segment was deposited at an applied potential of –100 mV, which is 80 mV lower than the applied potential for the Bi_2Te_3 segment. Such a high cathodic potential can lead to reduction of the crystal sizes of the BiSbTe phase.

In conclusion, we demonstrated for the first time, a facile technique to synthesize superlattice $Bi_2Te_3/(Bi_{0.3}Sb_{0.7})_2Te_3$ nanowires. The composition and length of each segment were precisely controlled by adjusting deposition potentials and times. Electrodeposition is a promising cost-effective technique to fabricate zero-dimensional thermoelectric superlattice nanowires with controlled dimensions. Thermoelectric properties of superlattice nanowires are currently under investigation.

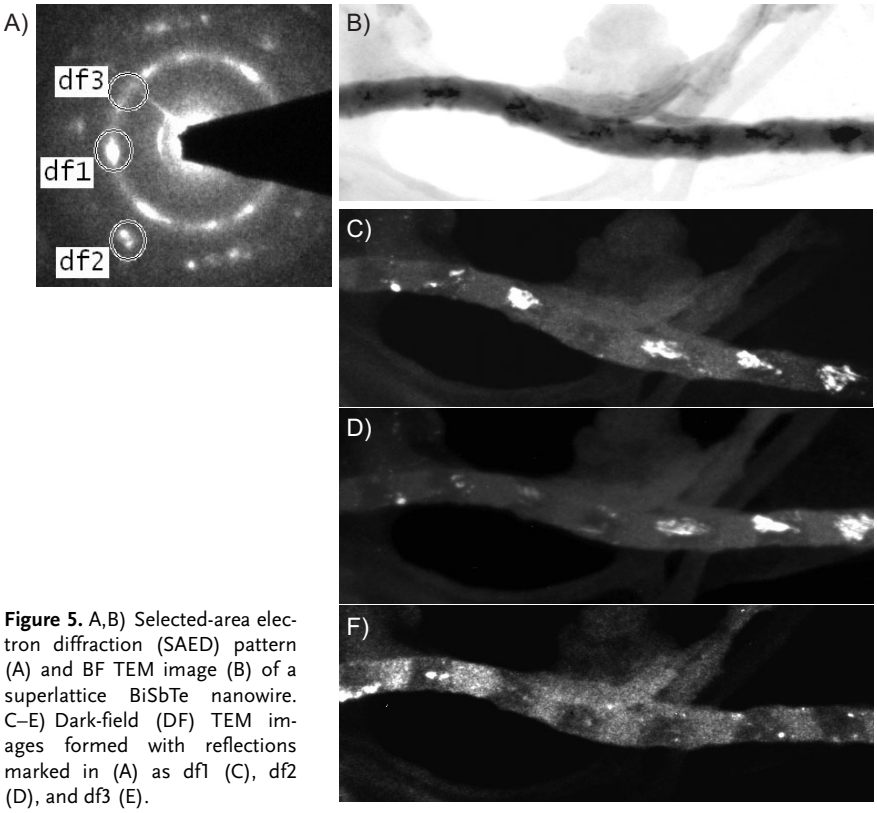

Figure 5. A,B) Selected-area electron diffraction (SAED) pattern (A) and BF TEM image (B) of a superlattice BiSbTe nanowire. C–E) Dark-field (DF) TEM images formed with reflections marked in (A) as df1 (C), df2 (D), and df3 (E).

Experimental

A tartaric–nitric electrolyte was prepared by first dissolving TeO_2 and $Bi(NO_3)_3{\cdot}5\,H_2O$ in concentrated nitric acid. Next, Sb_2O_3 was dissolved in a separate beaker by using 0.33 M tartaric acid as a complexing agent to improve the solubility of Sb in water through the formation of a Sb-tartaric complex. Once the solids were dissolved, the solutions were mixed and water was added to reach the final volume. The final electrolyte composition was 0.1 mM of Bi^{+3}, 1.6 mM SbO^{+}, 0.7 mM $HTeO_2^{+}$, and 33 mM tartaric acid in 1 M HNO_3.

Prior to electrodeposition, LSV measurements were performed to determine the deposition-potential range. Voltammetric experiments were conducted in a conventional three-electrode cell configuration at room temperature. Evaporated gold/chromium (3000 Å/300 Å thick) on a silicon substrate was used as a working electrode. Pt-coated titanium and a SCE were used as a counter and reference electrode, respectively. The scan rate was fixed at 10 $mV\,s^{-1}$. The solution was unstirred. After electroanalytical studies, the influence of the deposition potential on deposition rate, film composition, and film morphology was studied to determine the optimum deposition conditions for each segment.

Based on thin-film studies, superlattice BiTe/BiSbTe nanowires were fabricated by using a template-directed method, with polycarbonate membranes as nanotemplates (Nuclepore, Tracketch membrane, Whatman, diameter 13 mm). The actual pore diameter of the nanotemplates was approximately 50 nm (nominal pore size 30 nm) [22]. Prior to electrodeposition, a thin gold layer was sputtered onto one side of the membrane to serve as a seed layer. Subsequently, conducting copper tapes were attached to the nanotemplates to create electrodes. After assembly, the electrodes were covered with an insulator (Microstop, Pyramid Plastics, Inc.), except for the deposition area. Electrodeposition of superlattice nanowires was also performed in three-electrode cell configuration at room temperature. To fabricate the superlattice nanowires, the deposition potential was modulated between –20 and –100 mV (vs. SCE) using a computer-aided potentiostat (Princeton Applied Research Potentionstat, VMP2) with a total deposition time of 30 min. After deposition, the polycarbonate membranes were selectively dissolved in dichloromethane (99.9 %, Acroseal) for 2 h at 40 °C. Suspended nanowires were collected by centrifuging. The nanowires were resuspended in isopropyl alcohol after rinsing with deionized water for several days.

The composition of the deposit was determined by using atomic absorption spectroscopy (AAS, Perkin–Elmer, Analyst 800) for the thin films and by electron dispersive spectroscopy (EDS, Phoenix, EDAX) for the nanowires. The lengths and diameters of the nanowires were determined by SEM (LEO 1550 VP FESEM). The microstructure of nanowires was investigated by TEM (FEI CM300), using electron diffraction and diffraction contrast.

Received: March 22, 2006
Revised: August 12, 2006
Published online: January 3, 2007

[1] L. D. Hicks, M. S. Dresselhaus, *Phys. Rev. B: Condens. Matter Mater. Phys.* **1993**, *47*, 12 727.
[2] R. Venkatasubramanian, E. Siivola, T. Colpitts, B. O'Quinn, *Nature* **2001**, *413*, 597.
[3] R. Venkatasubramanian, T. Colpitts, E. Watko, M. Lamvik, N. El-Masry, *J. Cryst. Growth* **1997**, *170*, 817
[4] A. Raab, G. Springholz, *Appl. Phys. Lett.* **2002**, *81*, 2457.
[5] Y.-M. Lin, M. S. Dresselhaus, *Phys. Rev. B: Condens. Matter Mater. Phys.* **2003**, *68*, 075 304.
[6] C. Dames, G. Chen, *J. Appl. Phys.* **2004**, *95*, 682.
[7] Y. Wu, R. Fan, P. Yang, *Nano Lett.* **2002**, *2*, 83.
[8] M. S. Gudiksen, L. J. Lauhon, J. Wang, D. C. Smith, C. M. Lieber, *Nature* **2002**, *415*, 617.
[9] M. T. Björk, B. J. Ohlsson, T. Sass, A. I. Persson, C. Thelander, M. H. Magnusson, K. Deppert, L. R. Wallebberg, L. Samuelson, *Nano Lett.* **2002**, *2*, 87.
[10] L. Piraux, J. M. George, J. F. Despres, C. Leroy, E. Ferain, R. Legras, K. Ounadjela, A. Fert, *Appl. Phys. Lett.* **1994**, *65*, 2484.
[11] J.-R. Choi, S. J. Oh, H. Ju, J. Cheon, *Nano Lett.* **2005**, *5*, 2179.
[12] W. Wang, Q. Huang, F. Jia, J. Zhu, *J. Appl. Phys.* **2004**, *96*, 615.
[13] M. S. Martin-Gonzalez, A. L. Prieto, R. Gronsky, T. Sands, A. M. Stacy, *Adv. Mater.* **2003**, *15*, 1003.
[14] M. S. Sander, R. Gronsky, T. Sands, A. M. Stacy, *Chem. Mater.* **2003**, *15*, 335.
[15] H. Yu, P. C. Gibbons, W. E. Buhro, *J. Mater. Chem.* **2004**, *14*, 595.
[16] M. S. Sander, A. L. Prieto, R. Gronsky, T. Sands, A. M. Stacy, *Adv. Mater.* **2002**, *14*, 665.
[17] D. D. Fari, S. Diliberto, N. Stein, C. Boulanger, J.-M. Lecuire, *Thin Solid Films* **2005**, *483*, 44.
[18] J. R. Lim, J. Whitacre, J.-P. Fleurial, C. K. Huang, M. A. Ryan, N. V. Myung, *Adv. Mater.* **2005**, *17*, 1488.
[19] B. Y. Yoo, C.-K. Huang, J. R. Lim, J. Herman, M. A. Ryan, J.-P. Fleurial, N. V. Myung, *Electrochim. Acta* **2005**, *50*, 4371.
[20] T. Caillat, M. Carle, J. P. Fleurial, H. Scherrer, S. Scherrer, *MRS Symp. Proc.* **1991**, *234*, 189.
[21] M. Paunovic, M. Schlesinger, *Fundamentals of Electrochemical Deposition*, Wiley, New York **1998**, Ch. 7, p. 109.
[22] C. Schönenberger, B. M. I. van der Zande, L. G. J. Fokkink, M. Henny, C. Schmid, M. Krüger, A. Bachtold, R. Huber, H. Birk, U. Staufer, *J. Phys. Chem. B* **1997**, *101*, 5497.

